Article

Consolidation of Calcium Carbonate Using Polyacrylamides with Different Chemistries

Jin Hau Lew [1],* , Paul F. Luckham [1] , Omar K. Matar [1] , Erich A. Müller [1] , Adrielle Sousa Santos [1] and Myo Thant Maung Maung [2]

[1] Department of Chemical Engineering, Imperial College London, London SW7 2AZ, UK; p.luckham01@imperial.ac.uk (P.F.L.); o.matar@imperial.ac.uk (O.K.M.); e.muller@imperial.ac.uk (E.A.M.); adryellesousasantos@gmail.com (A.S.S.)

[2] PETRONAS Research Sdn. Bhd., Bandar Baru Bangi 43000, Selangor, Malaysia; maungmyothant@petronas.com

* Correspondence: s.lew20@imperial.ac.uk

Abstract: In this work, the consolidation of calcium carbonate ($CaCO_3$) by polyacrylamide (PAM) of different molecular weights, charge densities, and functional groups was investigated via oscillatory rheology and unconfined compressive strength (UCS) analysis. Oscillatory rheology showed that the storage modulus G' was approximately 10 times higher than the loss modulus G'', indicating a highly elastic $CaCO_3$ sample upon consolidation via PAM. Both oscillatory rheology and UCS analysis exhibited similar trends, wherein the mechanical values (G', G'', and UCS) first increased with increasing polymer dosage, until they reached a peak value (typically at 3 mgpol/g$CaCO_3$), followed by a decrease in the mechanical values. This indicates that there is an optimum polymer dosage for the different PAM-$CaCO_3$ colloidal systems, and that exceeding this value induces the re-stabilisation of the colloidal system, leading to a decreased degree of consolidation. Regarding the effect of the PAM molecular weight, the peak G' and UCS values of $CaCO_3$ consolidated by hydrolysed PAM (HPAM) of different molecular weights are very similar. This is likely due to the contour length of the HPAMs being either almost the same or longer than the average distance between two $CaCO_3$ particles. The effect of the PAM charge density revealed that the peak G' and UCS values decreased as the charge density of the PAM increased, while the optimum PAM dosage increased with decreasing PAM charge density. The higher likelihood of lower-charge PAM bridging between the particles contributes to higher elastic energy and mechanical strength. Finally, regarding the PAM functional group, $CaCO_3$ consolidated by sulfonated polyacrylamide (SPAM) typically offers lower mechanical strength than that consolidated with HPAM. The bulky sulfonate side groups of SPAM interfere with the surface packing, reducing the number of polymers able to adsorb onto the surface and, eventually, reducing the degree of consolidation of $CaCO_3$. The zeta potential of the PAM-$CaCO_3$ samples became more negative with increasing PAM concentration due to the saturation of the particle surface. Good agreement between oscillatory rheology and UCS analysis could accelerate PAM screening for optimum $CaCO_3$ consolidation.

Keywords: polyacrylamide; calcium carbonate; consolidation; molecular weight; charge density; functional group; unconfined compression stress; oscillatory rheology

1. Introduction

Approximately 60% of global natural gas reserves are found in carbonate reservoirs [1,2]. However, many of these carbonate reservoirs have not undergone sufficient natural cementation via the deposition of minerals [3], making these reservoirs weak and poorly consolidated [4], with weak rock formations that are vulnerable to collapse. As these rocks deform and collapse, they are crushed, leading to the production of fines also known as sanding [5], which could potentially lead to a reduction in hydrocarbon production, the failure of processing equipment, and an increased cost of operation due to fine disposal [6]. To address

this operational challenge, one common technique for formation strengthening involves the introduction of specific chemicals into the reservoir to bind the loose rock grains into stronger mass [7]. It is commonly known that colloidal systems can be stabilised due to the presence of an electrical double layer (EDL) of individual particles exerting repulsive force on one another. However, the colloids can be destabilised by the addition of polymers, and polyacrylamide (PAM) is one such polymer. After adsorbing onto a surface, PAM molecules can interact with neighbouring colloidal particles via a combination of bridging and patch attraction [8]. Polymers with a higher molecular weight or lower charge density will have a higher probability of adopting bridging interaction [9,10], whereas polymers of a lower molecular weight or higher charge density will be more likely to adopt patch attraction [11]. Atomic force microscopy of the adsorption of PAM with different molecular weights onto calcite crystal from our previous study also revealed a similar conclusion [12]. Colloidal particles that experience attraction due to polymers will aggregate into larger flocs. This aggregation increases with polymer concentration until an optimum concentration is reached. Beyond this optimum concentration, the polymer will continue to adsorb, resulting in a charge reversal of the particles and a re-stabilisation of the system; hence, very little or no aggregation of particles could be observed [13,14]. Such a concept of particle consolidation was explored by Lee, where he investigated the sequential application of oppositely charged PAM to enhance the agglomeration of loose sandstone particles [6]. Here, considerable success was demonstrated in increasing the agglomerate size, first by adding cationic PAM to agglomerate the negatively charged loose sand particles into micro-flocs, followed by adding anionic PAM to further bind the micro-flocs into larger flocs.

For quick identification of the strength profile of a rock sample, the unconfined compressive strength (UCS) test is typically recommended. Ideally, the compression test should be conducted on actual core plug samples. Core plug samples are usually small cylindrical samples that range between 25 and 38 mm in diameter, and their length is typically 1–1.5 times greater than the diameter. Sometimes, this ratio can even be 1–3 times [15]. However, as core plug samples are typically extracted directly from a well, these samples usually involve costly coring and extraction operations. Therefore, self-fabricated surrogate plug samples become desirable for chemical screening. For this purpose, a series of techniques to synthesise calcium carbonate ($CaCO_3$) plug samples have been published. One simple plug construction technique has been reported by Arismendi Florez et al. [16], involving compressing a $CaCO_3$–water mixture in a mould to form a usable carbonate plug. Inspired by them, we modified their technique to fabricate our plug samples for the sole purpose of studying the consolidation effect of various anionic polyacrylamides (PAMs). This method involves the mixing of calcium carbonate powder with PAM at certain ratios to form a thick slurry, which then is poured into a cylindrical mould for drying to obtain a plug. Ozhan [17] reported an adaptation of this method in his study of the consolidation of bentonite-sand mixture using anionic and cationic PAM. Similar to Arismendi, the plug samples in Ozhan's work involved the mixing of bentonite sand with PAM in a specific ratio, in which the wet paste was poured into a cylindrical mould, resulting in the formation of plug samples with the dimensions: diameter, 35 mm and height, 80 mm. The specimens were dried and subjected to uniaxial compression at 0.01 mm/min. Ozhan noted a swift increase in UCS as the concentration of PAM increased up to 2%; however, the rate of UCS increase became less pronounced beyond 2%. Ozhan attributed this UCS enhancement to the PAM molecules' ability to facilitate strong interactions between the PAM chains and the bentonite-sand particles, allowing the PAM molecules to effectively bind the particles together.

During the preparation of plug samples, a concentrated calcium carbonate ($CaCO_3$) suspension is obtained. The understanding of the viscoelastic properties of the suspension provides useful insight into the polymer's consolidation ability. Liang et al. studied the viscoelastic property of a concentrated sterically stabilised polystyrene latex dispersion via depletion flocculation via the addition of non-adsorbing polyethylene oxide (PEO) [18]. In their work, they observe that the storage modulus (G′) of the latex dispersion increases

with the increasing concentration of PEO added into it, until the G′ value plateaus. They proposed that the depletion flocculation of latex particles by non-adsorbing PEO increases with increasing PEO concentration, which, in turn, increases the magnitude of G′. This continues until a three-dimensional network structure is formed, hence limiting any further increase in G′. Thus, they suggested that G′ is predominantly dictated by the number of contacts formed between the flocculated units, rather than the strength of the structural unit formed. Although the anticipated polymer–substrate interaction in our work is different from that in the work of Liang et al. (20), it is still beneficial to gain some insights into the effect of the adsorbent concentration on the overall consolidation of the substrate. A similar concept was explored by Luckham et al. [19]; they studied the flocculation of concentrated dispersion of large negatively charged polystyrene particles (P−) via the addition of small positively charged polystyrene particles (P+). Their rheological results show that with increasing P+ concentration, the measured rheological parameters, including the shear modulus, increase until reaching a maximum, whereby further increases in P+ concentration only reduce the magnitude of the measured rheological parameters. They proposed that the extent of flocculation of P− increases with increasing P+ concentration until reaching a maximum, where the system restabilizes at a sufficiently high P+ concentration. A plausible explanation for the relationship between polymer configuration and the elastic property of samples is provided by Otsubo [20]. The author explained that if a single polymer may be able to bridge onto multiple particles, then this long-range interaction will increase the density of the flocs. These long-range bridges could contribute to high energy storage, which will then translate into a high storage modulus. Polymers with a higher probability of interacting through bridging interaction, either higher-molecular-weight or lower-charge polymers, are likely to experience such phenomena. On the other hand, if the polymer adopts a flatter configuration, he proposed that each bridge is independently and randomly distributed; thus, this lack of connectivity does not transmit high elasticity throughout the system. Thus, a colloidal system with polymers that encourage a more patch-like behaviour, such as those with a lower molecular weight or higher charge, usually have a lower elastic modulus.

Combining with our prior findings that polyacrylamide (PAM) readily adsorbs onto calcium carbonate ($CaCO_3$) [21], in this work, we seek to further explore the consolidation of $CaCO_3$ through the application of PAMs of different chemistry, i.e., different molecular weight, charge density, and functional group. Here, we propose a simple $CaCO_3$ plug fabrication technique, inspired by Arismendi Florez et al. [16], wherein we mixed $CaCO_3$ with PAM to form a thick paste. We conducted oscillatory rheometry on the thick paste formed and subsequently subjected the self-fabricated plugs to an unconfined compression stress (UCS) test to compare the efficacy of different PAMs regarding their consolidating ability toward $CaCO_3$. Zeta potential analysis on the PAM-$CaCO_3$ system was also conducted. To the best of our knowledge, a study of PAM's consolidation of $CaCO_3$ via comparing UCS and oscillatory shear rheology has not been investigated; thus, a successful comparison between these two parameters could significantly accelerate polymer screening before its application in an oil and gas field.

2. Materials and Methods

2.1. Materials

The calcium carbonate powder ($CaCO_3$, ≥99%) used in this work was purchased from VWR Chemicals Ltd. (Lutterworth, UK). To study the effect of the polyacrylamide (PAM) chemistry on $CaCO_3$ consolidation, the PAMs used in this study were hydrolysed polyacrylamide (HPAM) of different molecular weight and charge density and sulfonated polyacrylamide (SPAM). The details of the PAMs used are listed in Table 1. All these PAMs were provided by SNF Floerger (Wakefield, UK).

Table 1. Information regarding the PAMs used.

Polymer	Type	Functional Group	Charge Density	Molecular Weight (MDa)
F3330S	HPAM	Carboxylate	25–30%	11–13
F3530S	HPAM	Carboxylate	25–30%	15–17
F3630S	HPAM	Carboxylate	25–30%	18–20
AN910	HPAM	Carboxylate	10%	11–13
AN945	HPAM	Carboxylate	40%	11–13
AN125	SPAM	Sulfonate	25%	8
AN132	SPAM	Sulfonate	32%	8

The chemical structures of hydrolysed polyacrylamide (HPAM) and sulfonated polyacrylamide (SPAM) are illustrated in Figure 1. All the polyacrylamides (PAMs) used in this work are anionic due to their negatively charged functional group. The parameters studied in this work, along with the PAMs involved, are: (a) effect of PAM molecular weight (F3330, F3530, F3630); (b) effect of PAM charge density (F3330, AN910, AN945); and (c) effect of PAM functional group (F3330, AN125, AN132). All PAM solutions were prepared using deionized water (DI, 18 MΩ), and the experiments were conducted in room conditions (25 °C, 1 atm).
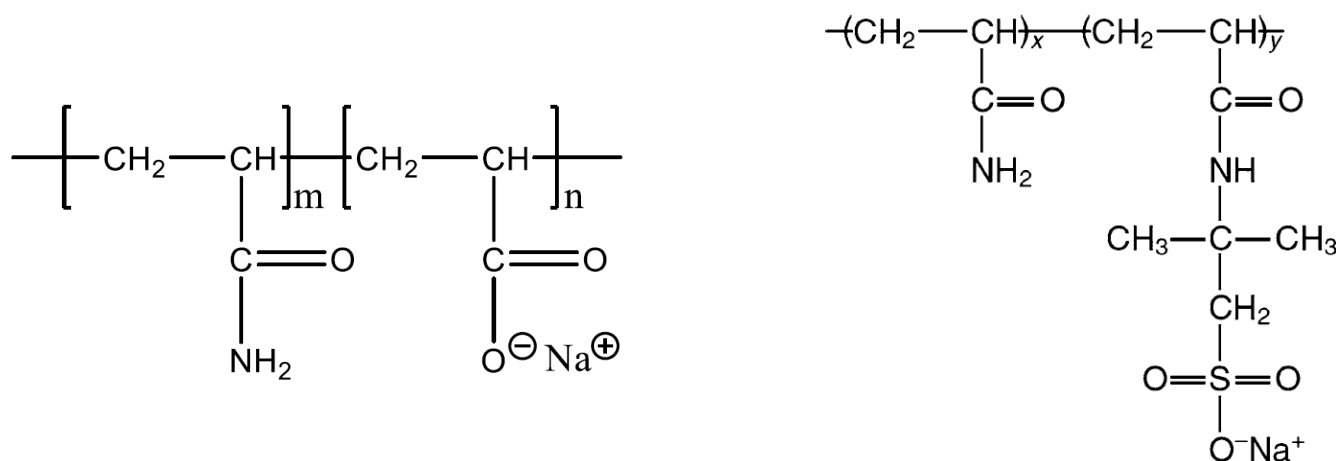
Figure 1. The molecular formula of hydrolysed polyacrylamide HPAM (**left**) and sulfonated polyacrylamide (SPAM) (**right**).

2.2. Experimental Procedures

2.2.1. Polymer and CaCO$_3$ Plug Sample Preparation

A 15,000 ppm mother stock polyacrylamide (PAM) solution was first prepared according to API-RP-63 using a magnetic stirrer (Thermo Fisher Scientific, Dartford, UK), with DI water as solvent. The solution was stirred for more than 24 h to achieve a homogeneous mother stock, which would then be diluted to PAM with concentrations ranging from 500 to 5000 ppm.

To prepare the CaCO$_3$ plug samples, a thick CaCO$_3$ paste was first prepared by mixing 60 g of CaCO$_3$ powder with 120 g of PAM solution. The sample was then stirred with an IKA EUROSTAR 60 overhead stirrer (IKA England Ltd., Oxford, UK) at 200 rpm for 1–2 h until a homogenous thick paste was obtained. A small amount of this thick paste was analysed for its oscillatory rheology, while the rest was poured into three separate cylindrical tubes to form cylindrical plug samples with dimensions of approximately 25 mm (D) × 50 mm (H). These samples were fan-dried, and their mass was recorded daily. The samples were deemed dried when the relative weight change was less than 5%. The entire experiment was then repeated, and another three sets of samples per polymer concentration were obtained. Thus, the average of a minimum of six samples was calculated. All the PAM concentrations in these experiments are reported in terms of milligrams of polymer per gram of carbonate, mgpol/gCaCO$_3$. Upon considering the CaCO$_3$ surface area and particle size from our previous work [21] in the calculation, 500 to 5000 ppm of PAM corresponds

to 1 to 10 mgpol/gCaCO$_3$. All the samples have a similar pH of approximately pH 9.5, regardless of PAM concentration. The variability in the volume per unit mass was also demonstrated from the F3330-CaCO$_3$ thick paste. Here, the mass of 5 mL of F3330-CaCO$_3$ thick paste was measured, which, in turn, allowed the calculation of the specific volume (cm^3/g) of the sample.

2.2.2. Oscillatory Rheology

A rheological study of the thick CaCO$_3$ paste was conducted using the Thermo-Fisher Haake MARS rotational rheometer (Thermo Fisher Scientific, Karlsruhe, Germany) fitted with a parallel plate geometry (P35, diameter of 50 mm and 1 mm gap). Oscillatory experiments were conducted to explore the viscoelastic nature of these pastes. Initially, an amplitude sweep experiment was conducted to determine the linear viscoelastic region (LVER). A frequency of 1 Hz was set, and the strain was set from 0.001% to 10%. The LVER is often found from a strain of 0.001% to 0.01%. An example is shown in Supplementary Material Figure S1. After obtaining the LVER, the strain was set to correspond to the LVER, and an oscillatory frequency sweep experiment was conducted, where the frequency ranged from 1 to 100 Hz. The storage modulus (G′) and loss modulus (G″) were measured as a function of the oscillatory frequency. The G′ and G″ were then plotted against the range of concentration of PAM.

2.2.3. Unconfined Compressive Strength (UCS) Test

The dried CaCO$_3$ plug samples were then subjected to UCS analysis using a Lloyds EZ50 uniaxial compression tester (AMETEK Test & Calibration Instruments, West Sussex, UK). A 1 kN load cell was used for the experiments, and the loading rate was maintained at 1 mm/min for all tests. Upon compression, the instrument generates a stress–strain curve. UCS is the highest stress the sample could be subjected to before fracture. A correction factor was applied to the final values obtained based on any variation in the diameter and length of each plug sample [15]. The corrected UCS, *C*, is calculated as:

$$C = \frac{C_a}{0.88 + \left(0.24\frac{D}{L}\right)} \tag{1}$$

where *D* and *L* are the diameter and length of the plug sample, respectively, and C_a is the measured UCS. The UCS was then plotted against the range of concentration of PAM.

2.2.4. Zeta Potential Analysis

The procedure for zeta potential analysis using the Anton Paar Litesizer 500 (Ostfildern, Germany) has been published in our previous work [21]. We invite readers to refer to that publication for detailed information.

3. Results

3.1. Effect of Polyacrylamide Molecular Weight on Calcium Carbonate Consolidation

Before the moduli and compiled unconfined compressive strength (UCS) are shown, an example stress–strain curve during the compression of the calcium carbonate (CaCO$_3$) plug samples is presented in Figure 2.

In Figure 2, the stress–strain curve of the CaCO$_3$ plug consolidated by F3330 solution at different polymer concentrations show that the samples experienced primarily shear failure. This is a common phenomenon observed in rock failure, especially if the sample is under anisotropic stress conditions, such as that in the UCS experiment [22]. The stress–strain curves for the CaCO$_3$ plug consolidated by every polymer used in this work are qualitatively identical; that is, they all show shear failure. Thus, we will not present the stress–strain curves again as they do not convey any added information. From the stress–strain curves, the peak stress represents the unconfined compressive stress (UCS), and the UCS values were compiled and presented (see Figure 3) for different polymers.

The effect of the hydrolysed polyacrylamide (HPAM) molecular weight on calcium carbonate ($CaCO_3$) consolidation was investigated by comparing F3330, F3530, and F3630. Before plotting G′ and G″ against HPAM concentration, we observed that the result from the oscillatory frequency sweep always showed a horizontal straight-line plot of G′ and G″ against the oscillatory frequency, regardless of HPAM concentration. This result further confirms that every measurement is conducted in the linear viscoelastic region (LVER). Examples of oscillatory frequency sweep plots of F3330 at low, medium, and high polymer concentration is shown in Figure S2, in which this trend is observed for every type of PAM used in our work. The G′ and G″ values were then averaged and plotted against the HPAM concentration, while the wet samples were then dried in cylindrical moulds, and the plug samples were crushed to obtain the unconfined compressive strength (UCS). The concentrations are in terms of mgpol/gCaCO₃. The moduli and UCS results are shown in Figure 3.
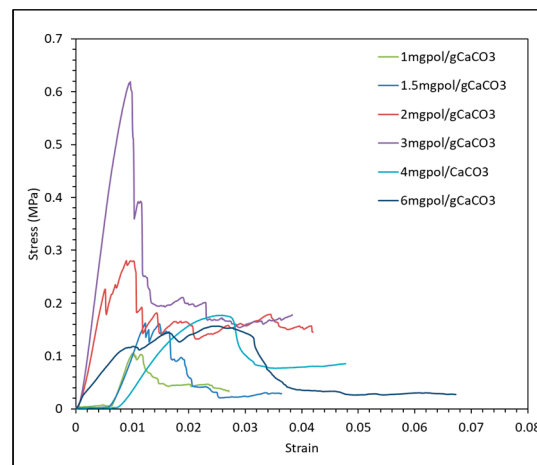
**Figure 2.** Stress–strain curve of CaCO3 consolidation by F3330.
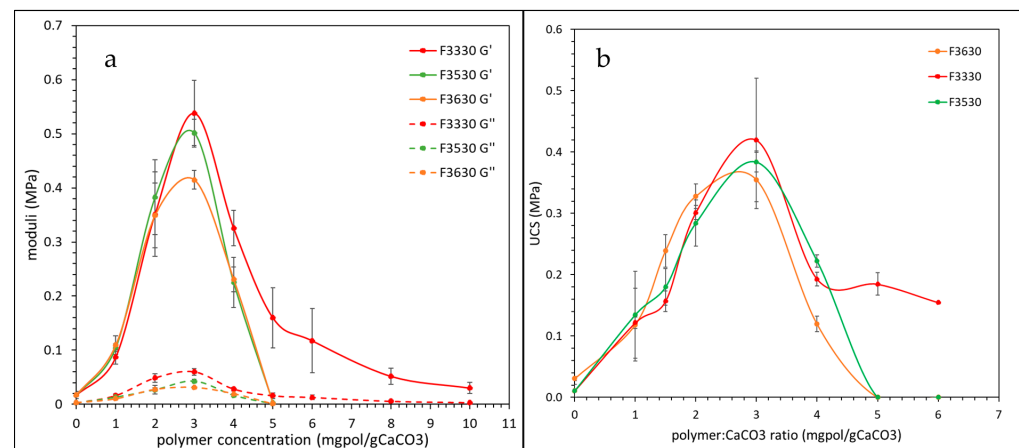
Figure 3. Effect of the HPAM molecular weight on (**a**) the storage modulus (G′) and loss modulus (G″); (**b**) the unconfined compressive stress (UCS) of consolidated $CaCO_3$ sample.

From Figure 3, we can see that the values of the storage modulus (G′) are significantly higher than the loss modulus (G″) and indicate very high elastic behaviour relative to viscous behaviour [23]. An observation from the moduli and UCS plot in Figure 3 is that the trends of both graphs are very similar; initially, there is an increase in the strength parameters (G′, G″, and UCS) with increasing HPAM dosage until they reach a peak value at 3 mgpol/gCaCO₃, followed by a decrease in these parameters. The G′ and UCS are within one order magnitude difference, which shows a very close correlation between the elastic modulus obtained at the linear viscoelastic region (LVER) and the final mechanical strength of the sample. Upon

adsorbing onto a surface, high-molecular polymers tend to form loops and tails that easily bridge onto neighbouring particles [24,25]. At low polymer concentrations, the polymer counts might not be sufficient to properly bridge between $CaCO_3$ particles, hence the lower magnitude observed. The peak value is observed at 3 mgpol/$gCaCO_3$ when there is a high degree of bridging of $CaCO_3$ by the HPAM molecules. Beyond 3 mgpol/$gCaCO_3$, we observed a clear display of the consequences of steric stabilisation due to overdosage of the polymer [26,27]. Above 3 mgpol/$gCaCO_3$, the surface of the initially positively charged $CaCO_3$ particles would have been slowly saturated by the HPAM molecules and would have begun to impose repulsive force on one another and gradually weaken the effect of polymer bridging [13]. Above 6 mgpol/$gCaCO_3$, the $CaCO_3$ could have been fully saturated by HPAM molecules, and there is a residual net repulsion between the particles, causing the steric restabilisation of the entire colloidal system. Above 6 mgpol/$gCaCO_3$, we noticed that most of the $CaCO_3$ paste fractured during the drying process, and we were unable to obtain any operable plug samples. Therefore, for such samples, we simply denoted their UCS to be 0 MPa. Pictures of functional samples obtained below 6 mgpol/$gCaCO_3$ and fractured plug samples obtained above 6 mgpol/$gCaCO_3$ are shown in Figure 4.
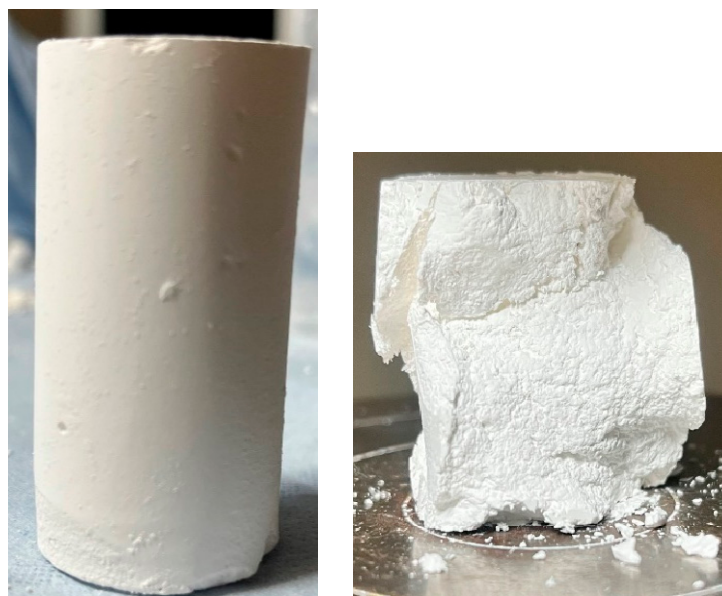
Figure 4. Functional plug sample obtained from 500–3000 ppm, or 1–6 mgpol/$gCaCO_3$ (**left**) and fractured plug sample obtained above 3000 ppm, or 6 mgpol/$gCaCO_3$ (**right**).

In our previous work [21], the adsorption isotherm showed that as the polymer molecular weight increases, the amount of polymer adsorbed also increases. However, in Figure 3, we can observe that all the measured mechanical parameters are very similar regardless of hydrolysed polyacrylamide (HPAM) molecular weight. We propose that this is mainly due to the volume fraction of $CaCO_3$ in both systems being very different; thus, the bridging of HPAM across two $CaCO_3$ particles in both systems is different. The $CaCO_3$-to-HPAM mass ratio in our previous work [21] was 1:25, whereas the ratio used here is 1:2, making the volume fraction of $CaCO_3$ in our previous [21] and current work 0.015 and 0.185, respectively. According to Mewis and Wagner [28], suspensions with a volume fraction below 0.1 are considered dilute suspensions, while suspensions with a volume fraction above 0.15 are considered to be a concentrated suspension. For concentrated suspensions, a further increase in solid fraction will lead to the formation of a paste, which is what was observed in this work. For clarity, we shall name the dilute suspension from our previous work [21] as a dilute system, and the current $CaCO_3$ paste as a concentrated system. The average diameter of a $CaCO_3$ particle measured from our previous work [21] was approximately 3.5 μm. Assuming all the $CaCO_3$ particles are packed in a 1 cm^3 cubic lattice structure, and assuming equidistant separation between two $CaCO_3$ particles, the

average separation distance between the dilute system and the concentrated system is 14.27 μm (or approximately 4 particle diameters) and 6.15 μm (or approximately 2 particle diameters), respectively. We visualise this arrangement in Figure 5.
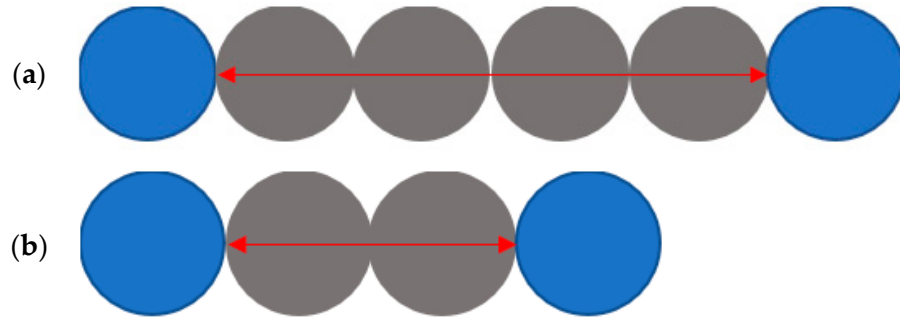

Figure 5. Illustration of the average distance between two CaCO$_3$ particles (blue) in a (**a**) dilute system and (**b**) concentrated system.

Next, we estimated the average length of each HPAM molecule. Assuming a bond angle of 120°, the formula to calculate the contour length, *L* of a polymer is given by:

$$L = \frac{MW_P}{MW_M} \times L_{C-C} \times \sin\left(\frac{\theta_B}{2}\right) \tag{2}$$

where MW_P and MW_M are the molecular weight of the polymer and monomer, respectively, L_{C-C} is the length of the carbon–carbon chain, and θ_B is the bond angle. The calculated MW_M for 30% acrylamide is 213 g/mol; thus, the contour length of the three polymers used are:

$$L_{F3330} = 6.9 \text{ μm}; L_{F3530} = 9.4 \text{ μm}; L_{F3630} = 12.5 \text{ μm}$$

It may be seen that the contour length of all three HPAMs is either the same or longer than the average distance between two CaCO$_3$ particles in the concentrated system. However, in the dilute system, the contour length is shorter than the average distance between two CaCO$_3$ particles and, in the case of F3330, the contour length did not even reach half of this distance. Thus, this might explain why in the concentrated system, the change in molecular weight of the HPAM used did not cause a significant difference in moduli (G′ and G″) and UCS value, yet a clear trend could be observed in the dilute system. An illustration of the possible bridging phenomenon in both the dilute system and the concentrated system is shown in Figure 6.
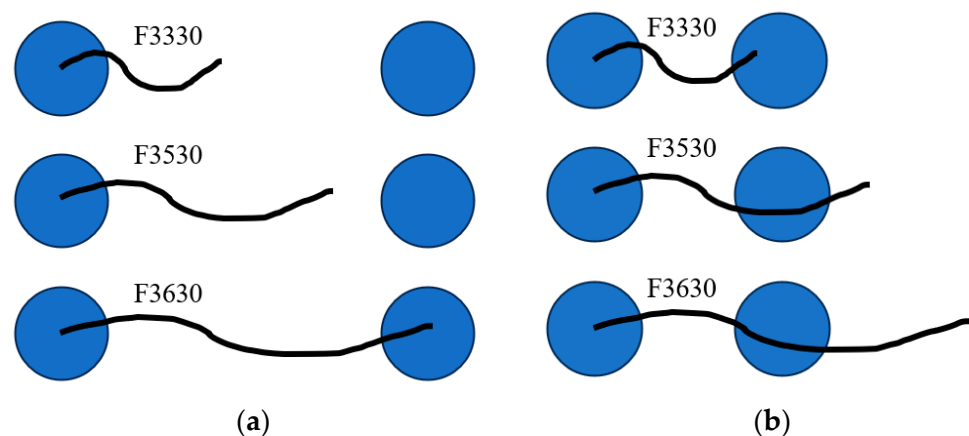

Figure 6. Possible bridging phenomenon in (**a**) a dilute system and (**b**) a concentrated system. Polymers are depicted as thick black lines, while spheres represent CaCO$_3$ particles.

The zeta potential of the HPAM-CaCO$_3$ colloidal system using HPAM of different molecular weights is shown in Figure 7.

The zeta potential result in Figure 7 has been published in our previous work [21]. We invite readers to refer to that publication for a more detailed explanation of the trend obtained. The zeta potential of all three HPAM–CaCO$_3$ mixtures becomes more negative as the HPAM concentration increases until a plateau is observed, and a transition from positive to negative zeta potential is observed between 0 and 1 mgpol/gCaCO$_3$. While CaCO$_3$ particles are typically positively charged in the absence of polymers due to having a point of zero charge (PZC) of 9.40–9.60 [29–31], the introduction of anionic HPAM will gradually neutralise the CaCO$_3$ surface positive charge. Above 1 mgpol/gCaCO$_3$, the continuous addition of HPAM will only further saturate the CaCO$_3$ surface with negatively charged HPAM and, eventually, the CaCO$_3$ will be fully saturated with HPAM and the repulsive forces will no longer increase; thus, a plateau in zeta potential will be observed [13].
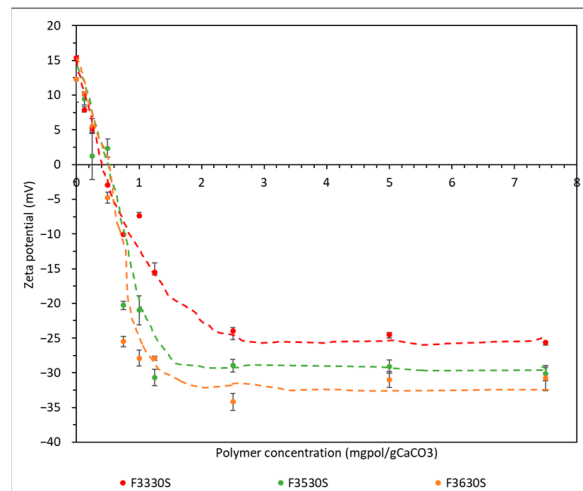
Figure 7. Zeta potential result for CaCO3 adsorbed with F3330S, F3530S, and F3630S.

An example of the effect of intermolecular bridging by polyacrylamide (PAM) on a specific volume of the PAM-CaCO$_3$ mixture was also calculated and is presented in Figure 8. Here, the F3330-CaCO$_3$ mixture was taken as an example.
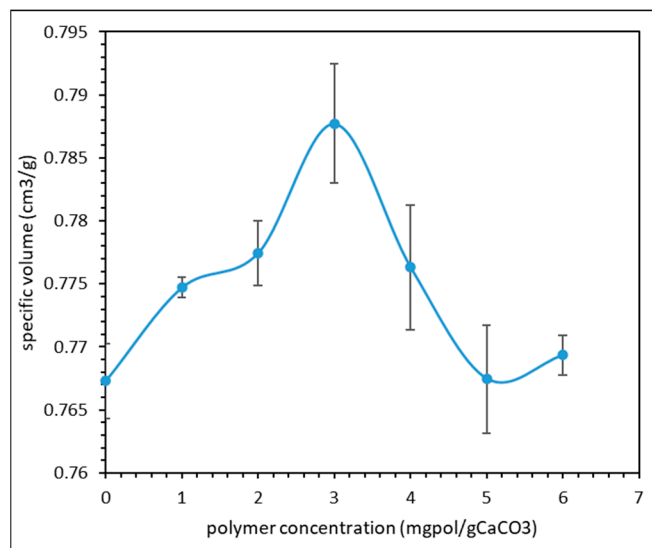

Figure 8. Specific volume of F3330-CaCO$_3$ mixture.

The results in Figure 8 display an identical trend to that obtained from Figure 3; the specific volume of the F3330-CaCO$_3$ mixture increases with increasing polymer concentration until a peak is reached at 3 mgpol/gCaCO$_3$. The increase in specific volume before 3 mgpol/gCaCO$_3$ is the result of interparticle bridging by F3330 molecules which forms larger aggregates that do not sediment properly, thus trapping more liquid pockets that result in a slightly larger bulk volume. Beyond 3 mgpol/gCaCO$_3$, the steric stabilisation due to an overdosage of the polymer might have discouraged the formation of larger aggregates; hence, the particles could sediment more compactly, leading to a decrease in specific volume [13,26,27].

3.2. Effect of Polyacrylamide Charge Density on Calcium Carbonate Consolidation

The effect of the hydrolysed polyacrylamide (HPAM) charge density on calcium carbonate (CaCO$_3$) consolidation was investigated by comparing F3330, AN910, and AN945. The oscillatory shear rheology and UCS results are shown in Figure 9.
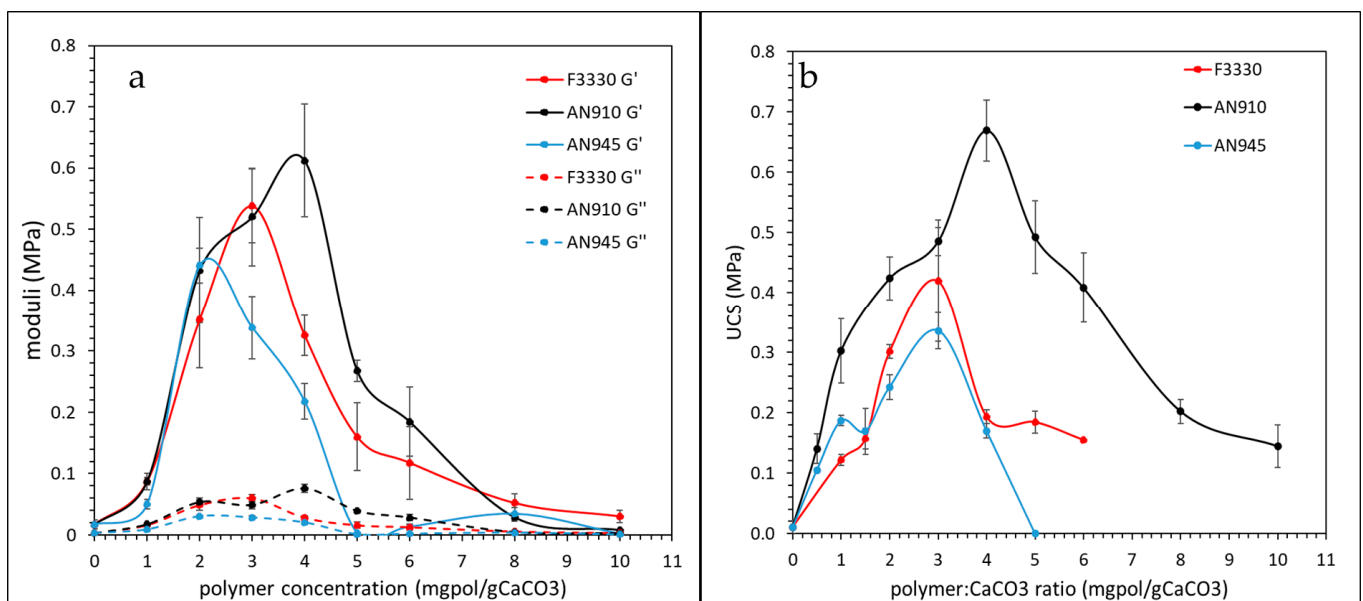
Figure 9. Effect of the HPAM charge density on (**a**) the storage modulus (G′) and loss modulus (G″); (**b**) the UCS of the consolidated CaCO$_3$ sample.

From this Figure 9, we observed again that the storage modulus (G′) is significantly higher than the loss modulus (G″), which shows that the CaCO$_3$ samples consolidated with HPAM are highly elastic. The first outcome that we observed from both moduli and UCS plots Figure 9 is that the magnitude of the mechanical parameters increased with decreasing polymer charge density. From the UCS plot, the overall UCS of samples consolidated by AN910 is larger than that by F3330 and AN945. According to Gan and Franks [32], lower-charge-density polymers have a higher likelihood of adopting bridging attraction, while higher-charge-density polymers are more likely to adopt patch attraction. This does not suggest that low-density polymers only exhibit bridging properties, while high-charge polymers only exhibit patch attraction. It simply suggests that there is a higher likelihood of polymer bridging by a lower-charged polymer than by a higher-charged polymer. Polymers more likely to form a bridging attraction typically have a larger number of protruding loops and tails than polymers favouring patch attraction, in which these typically lie flat on a substrate surface. The protruding loops and tails of low-charge-density polymers have a higher probability of bridging onto multiple particles, and these long-range bridges contribute to higher energy storage, which also translates to increased mechanical strength. Higher-charge-density polymers that lie flat on a surface lack such connectivity, causing a lower elasticity throughout the system [20]. Another observation is that the polymer dosage

that results in peak mechanical value increases with a decreasing HPAM charge density. We can observe from the moduli plot that AN910 requires 4 mgpol/gCaCO$_3$ to achieve peak moduli, followed by 3 mgpol/gCaCO$_3$ by F3330 and 2 mgpol/gCaCO$_3$ by AN945. The UCS result also showed that the polymer dosage that gives peak UCS is higher in AN910 than in F3330 and AN945. Such a trend is logical since a higher-charge-density polymer has a higher probability of adopting patch attraction and could cover a given surface quicker than a lower-charge polymer, thus causing faster charge stabilisation [25,33]. Similar findings were observed in Yang and Franks's work [32], where a higher-charged cationic polymer requires a lesser dosage to achieve optimum consolidation than lower-charged ones. Zhou et al. also mentioned that the charge density is more influential than the molecular weight of the polymer regarding aggregation mechanisms and properties [25], which explains why a clear difference could be observed in Figure 9 compared to that due to the HPAM molecular weight in Figure 3.

In Figure 10, the trend in zeta potential shows that with an increasing anionic polymer charge density, the zeta potential of the colloidal system becomes more negative. This trend is within expectations, as higher-charge-density polymers adsorb more onto the adsorbent surface, so will induce a higher negative charge [34]. Thus, AN945, as the highest-charged polymer among the three, shows the fastest reduction in zeta potential and the most negative zeta potential plateau among the three. On the other hand, the decrement in zeta potential for AN910, the lowest-charged polymer, has a gentler slope, and the plateau zeta potential is also the least negative.
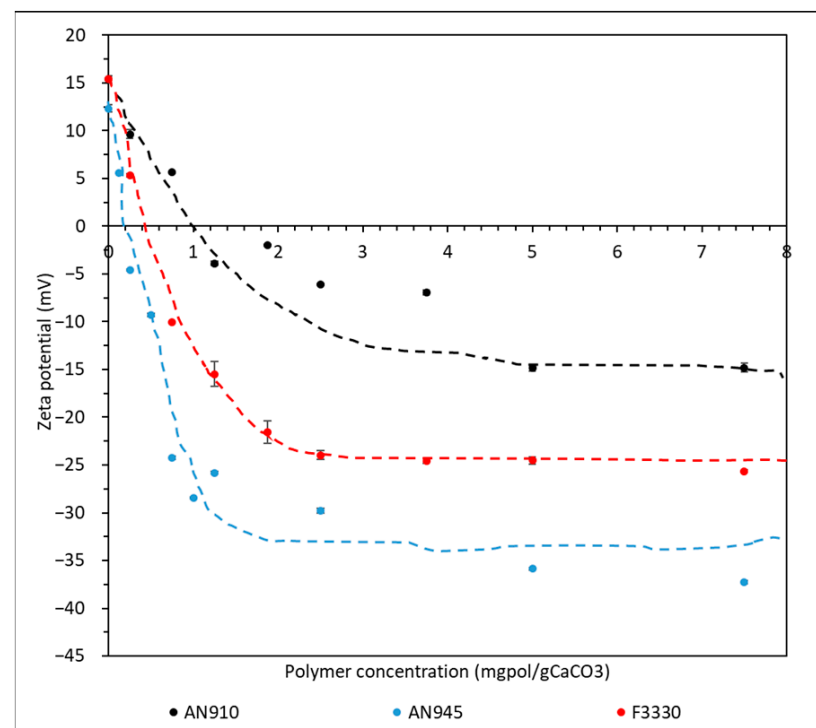

Figure 10. Zeta potential results for CaCO3 adsorbed with F3330S, AN910, and AN945.

3.3. Effect of Polyacrylamide Functional Group on Calcium Carbonate Consolidation

The effect of the polyacrylamide (PAM) functional group on calcium carbonate (CaCO$_3$) consolidation was investigated by comparing between F3330, AN125, and AN132. AN125 and AN132 are sulfonated polyacrylamides (SPAMs); thus, they have a different functional group than F3330, which is a hydrolysed polyacrylamide (HPAM). The oscillatory shear rheology and UCS results are shown in Figure 11.
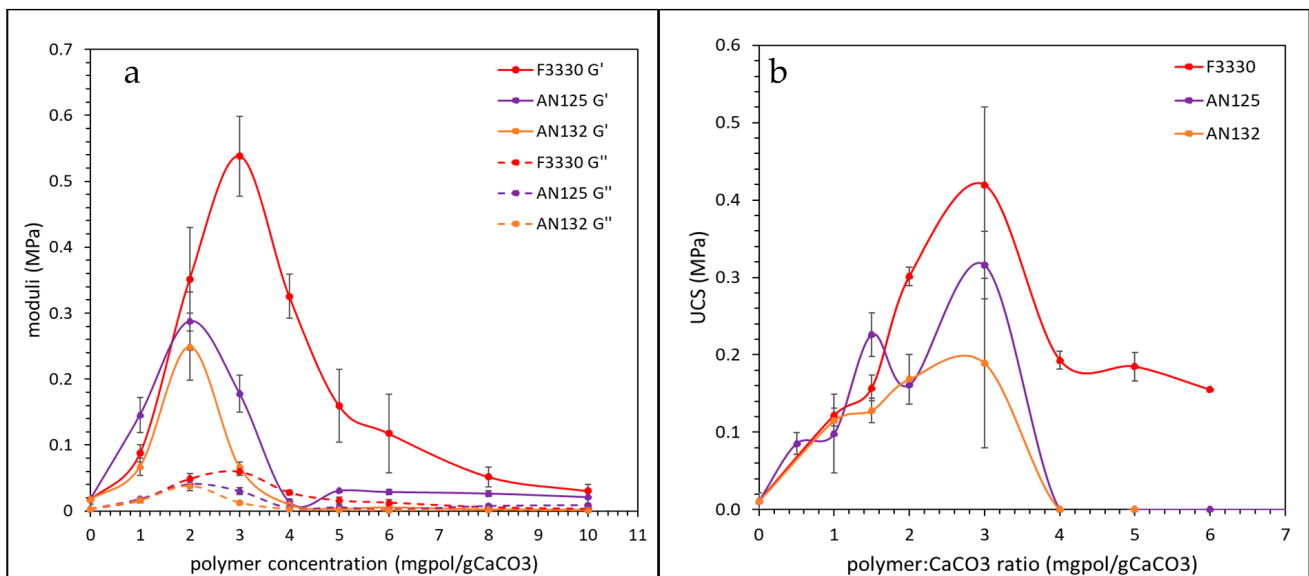
Figure 11. Effect of the PAM functional group on (**a**) the storage modulus (G′) and loss modulus (G″); (**b**) the UCS of the consolidated CaCO$_3$ sample.

From Figure 11, we again observed high sample elasticity, shown by the significantly higher storage modulus (G′) relative to the loss modulus (G″). The key observation from Figure 11 is that the magnitude of the mechanical parameters of CaCO$_3$ consolidated by hydrolysed polyacrylamide (HPAM) is generally higher than that by sulfonated polyacrylamide (SPAM); this trend is more obvious from the oscillatory moduli plot in Figure 11. This is very likely due to the presence of a bulky sulfonate group of SPAM interfering with the surface packing, thus reducing the amount of polymer able to adsorb onto the surface [35,36]. Lower polymer adsorption also signifies a lower degree of consolidation of CaCO$_3$ by SPAM. Comparable results were also reported by Plank and Bernhard in their work on α-Allyl-ω-methoxypolyethylene glycol-maleic anhydride copolymer adsorption onto cement. They noticed a rapid decrease in polymer adsorption with increasing side-chain length, which was attributed to the higher surface occupancy of the larger side group leading to hindrance in adsorption [37]. We observed a similar trend in our related work, where umbrella sampling free adsorption energy analysis using molecular dynamic (MD) simulations also revealed that HPAM has higher adsorption-free energy than SPAM [38]. The difference in magnitude of moduli and UCS between AN125 and AN132 is not significant, as these two SPAMs have similar charge densities. On the other hand, while the SPAM dosages that give the peak UCS and moduli are slightly different, we believe this observation is insignificant, given the large error bars for the UCS of SPAM at 3 mgpol/gCaCO$_3$. It is also noteworthy to mention that the final polymer concentration upon drying will slightly increase, which might play a part in further consolidating the CaCO$_3$ sample. The most important outcome we can obtain from these results is that the SPAM-consolidated CaCO$_3$ typically exhibits lower mechanical parameters than the ones where HPAM is employed.

Figure 12 shows that the zeta potential of all three polyacrylamides is very similar. It is surprising to see that both SPAMs (AN125 and AN132) share an almost-similar trend and plateau zeta potential value with HPAM (F3330S), even though the adsorption of SPAMs onto CaCO$_3$ should be significantly lower than that of HPAM. Plank and Bernhard also noticed similar zeta potential behaviour in their work, where the polymers with larger side chains brought about a more significant change in zeta potential despite having lower adsorbed amounts than polymers with smaller side chains. They attributed this phenomenon to the steric effect of the larger side chains moving the shear plane of the zeta potential further away from the positively charged particle surface, resulting in an apparent decrease in zeta potential [37]. Thus, the large, sulfonated side chain may move the shear

plane of zeta potential slightly further away from the $CaCO_3$ surface, thus imposing an apparent negative charge measurement on the instrument.
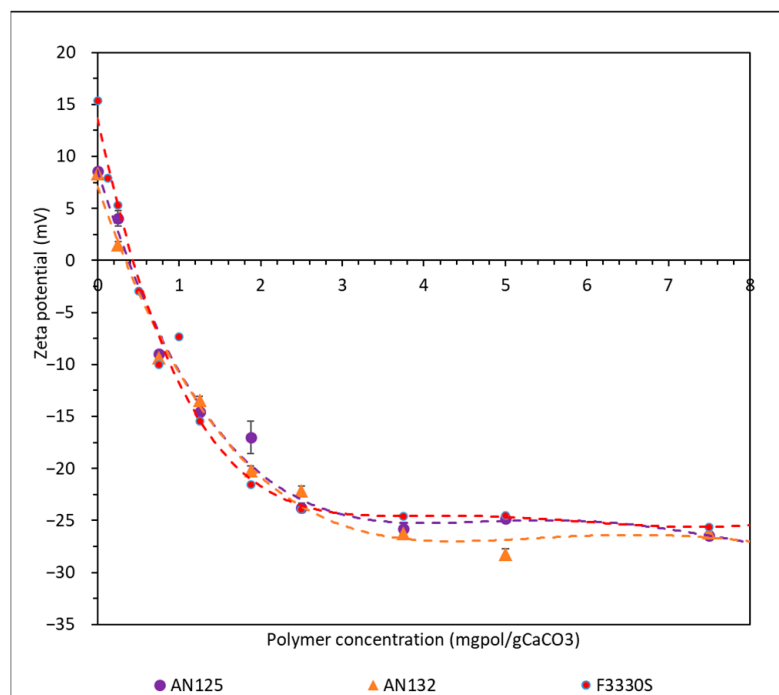

Figure 12. Zeta potential results for $CaCO_3$ adsorbed with F3330S, AN125, and AN132.

4. Conclusions

In this work, the consolidation of calcium carbonate ($CaCO_3$) by polyacrylamide (PAM) with different chemistries was investigated via oscillatory rheology and unconfined compressive strength analysis. Oscillatory rheology showed that the storage modulus G' is always significantly higher than the loss modulus G'', which indicates that the $CaCO_3$ consolidated by PAM is highly elastic. Good agreement between the trends seen in the oscillatory rheology and the UCS analysis is consistently observed in every experiment. We observed that as the PAM dosage increased, the consolidated $CaCO_3$ samples showed increasing mechanical properties until they reached a peak value, and then a drop in the magnitude of mechanical properties followed. The consistency of this trend showed that there is an optimum polymer dosage and that exceeding this value will cause the re-stabilisation of the colloidal system, leading to a decreased degree of consolidation. The mechanical properties of $CaCO_3$ consolidated by hydrolysed PAM (HPAM) of different molecular weights showed little difference. We explain this behaviour by estimating that the contour length of all three HPAMs is either almost the same or longer than the average distance between two $CaCO_3$ particles. Oscillatory rheology and UCS analysis revealed that $CaCO_3$ consolidated by HPAM of a lower charge density had higher mechanical strength. Lower-charge-density polymers have a higher probability of adopting bridging attraction due to the protruding loops and tails bridging onto multiple $CaCO_3$ particles, contributing to higher energy storage, and thus increasing mechanical strength. Finally, $CaCO_3$ consolidated by sulfonated polyacrylamide (SPAM) typically has lower mechanical strength than that consolidated with HPAM. SPAM includes bulky sulfonate side groups that interfere with the surface packing, reducing the number of polymers able to adsorb onto the surface and eventually reducing the degree of consolidation of $CaCO_3$. The good agreement between oscillatory rheology and the UCS experiment meant that PAM screening could be accelerated with a small number of samples and a short amount of time. Zeta potential analysis was also included to further support oscillatory rheology and UCS results. While the current results show that PAM has good consolidation capability in room conditions, the literature suggests that there is potential degradation in harsh

reservoir conditions. The degradation of PAM might lead to membrane fouling in oil and gas applications [39], while the degradation of PAM into its acrylamide monomer could also harm aquatic life due to being neurotoxic and carcinogenic [40,41]. Therefore, the next phase of the study is to investigate the consolidation ability of PAM in reservoir conditions and to propose suitable PAM enhancement techniques to reduce the degradation of PAM in these reservoir conditions.

References

1. Wang, S.; Li, G.; Li, Y.; Guo, J.; Zhou, S.; Yong, S.; Pan, B.; Bai, B. Adsorption of new hydrophobic polyacrylamide on the calcite surface. *J. Appl. Polym. Sci.* **2017**, *134*, 45314–45321. [CrossRef]
2. Mahmood, A.; Vissapragada, B.; Alghamdi, A.H.; Allen, D.; Herron, M.; Carnegie, A.; Dutta, D.; Olesen, J.-R.; Chourasiya, R.D.; Logan, D.; et al. A Snapshot of Carbonate Reservoir Evaluation. *Oilfield Rev.* **2000**, *12*, 20–41.
3. Talaghat, M.R.; Esmaeilzadeh, F.; Mowla, D. Sand production control by chemical consolidation. *J. Pet. Sci. Eng.* **2009**, *67*, 34–40. [CrossRef]
4. Nouri, A.; Vaziri, H.; Belhaj, H.; Islam, R. Effect of Volumetric Failure on Sand Production in Oil-Wellbores. SPE 80448. In Proceedings of the SPE—Asia Pacific Oil and Gas Conference and Exhibition, Jakarta, Indonesia, 9–11 September 2003; pp. 86–93.
5. Gun, W.J.; Routh, A.F.; Aytkhozhina, D.; Aston, M. Sand consolidation via latex destabilization. *AIChE J.* **2017**, *63*, 2610–2617. [CrossRef]
6. Lee, R.Y. Development of Sand Agglomeration Formulation for Oil & Gas Well Applications to Reduce the Production of Fine Particulates. Ph.D. Thesis, Imperial College London, London, UK, 2019.
7. Samarkin, Y.; Aljawad, M.S.; Amao, A.; Solling, T.; Abu-Khamsin, S.A.; Patil, S.; AlTammar, M.J.; Alruwaili, K.M. Carbonate Rock Chemical Consolidation Methods: Advancement and Applications. *Energy Fuels* **2022**, *36*, 4186–4197. [CrossRef]
8. Dixon, D.V.; Soares, J.B.P. Molecular weight distribution effects of polyacrylamide flocculants on clay aggregate formation. *Colloids Surf. A Physicochem. Eng. Asp.* **2022**, *649*, 129487. [CrossRef]
9. Rice, S.A.; Nagasawa, M. *Polyelectrolyte Solutions, a Theoretical Introduction*; Academic Press: London, UK, 1961.
10. Caskey, J.A.; Primus, R.J. The effect of anionic polyacrylamide molecular conformation and configuration on flocculation effectiveness. *Environ. Prog. Sustain. Energy* **1986**, *5*, 98–103. [CrossRef]
11. Fleer, G.J. Polymers at interfaces and in colloidal dispersions. *Adv. Colloid Interface Sci.* **2010**, *159*, 99–116. [CrossRef]

12. Lew, J.H.; Matar, O.K.; Müller, E.A.; Luckham, P.F.; Sousa Santos, A.; Myo Thant, M.M. Atomic Force Microscopy of Hydrolysed Polyacrylamide Adsorption onto Calcium Carbonate. *Polymers* **2023**, *15*, 4037. [CrossRef]

13. Szilagyi, I.; Trefalt, G.; Tiraferri, A.; Maroni, P.; Borkovec, M. Polyelectrolyte adsorption, interparticle forces, and colloidal aggregation. *Soft Matter* **2014**, *10*, 2479–2502. [CrossRef]

14. Gregory, J.; Barany, S. Adsorption and flocculation by polymers and polymer mixtures. *Adv. Colloid Interface Sci.* **2011**, *169*, 1–12. [CrossRef]

15. Thuro, K.; Plinninger, R.; Zah, S.; Schutz, S. Scale effects in rock strength properties. Part 1: Unconfined compressive test and Brazilian test. In *Rock Mechanics, a Challenge for Society*; Swets & Zeitlinger: Lisse, The Netherlands, 2001; pp. 169–174.

16. Arismendi Florez, J.J.; Ferrari, J.V.; Michelon, M.; Ulsen, C. Construction of synthetic carbonate plugs: A review and some recent developments. *Oil Gas Sci. Technol. Rev. IFP Energ. Nouv.* **2019**, *74*, 29. [CrossRef]

17. Özhan, H. Determination of mechanical and hydraulic properties of polyacrylamide-added bentonite-sand mixtures. *Bull. Eng. Geol. Environ.* **2021**, *80*, 2557–2571. [CrossRef]

18. Liang, W.; Tadros, T.F.; Luckham, P.F. Investigations of Depletion Flocculation of Concentrated Sterically Stabilized Latex Dispersions Using Viscoelastic Measurements and Microscopy. *J. Colloid Interface Sci.* **1993**, *158*, 152–158. [CrossRef]

19. Luckham, P.F.; Vincent, B.; Tadros, T.F. The controlled flocculation of particulate dispersions using small particles of opposite charge. IV. Effect of surface coverage of adsorbed polymer on heteroflocculation. *Colloids Surf.* **1983**, *6*, 119–133. [CrossRef]

20. Otsubo, Y. Effect of particle size on the bridging structure and elastic properties of flocculated suspensions. *J. Colloid Interface Sci.* **1992**, *153*, 584–586. [CrossRef]

21. Lew, J.H.; Matar, O.K.; Müller, E.A.; Maung, M.T.M.; Luckham, P.F. Adsorption of Hydrolysed Polyacrylamide onto Calcium Carbonate. *Polymers* **2022**, *14*, 405. [CrossRef] [PubMed]

22. Dusseault, M.B.; Collins, P.M. Geomechanics Effects in Thermal Processes for Heavy-Oil Exploitation. In *Heavy Oils: Reservoir Characterization and Production Monitoring*; Geophysical Developments Series; Society of Exploration Geophysicists: Houston, TX, USA, 2010; pp. 287–291.

23. Salehi, M.B.; Moghadam, A.M.; Marandi, S.Z. Polyacrylamide hydrogel application in sand control with compressive strength testing. *Pet. Sci.* **2019**, *16*, 94–104. [CrossRef]

24. Rabiee, A. Acrylamide-Based Anionic Polyelectrolytes and Their Applications: A Survey. *J. Vinyl Addit. Technol.* **2010**, *16*, 111–119. [CrossRef]

25. Zhou, Y.; Yu, H.; Wanless, E.; Jameson, G.; Franks, G.V. Influence of polymer charge on the shear yield stress of silica aggregated with adsorbed cationic polymers. *J. Colloid Interface Sci.* **2009**, *336*, 533–543. [CrossRef]

26. Wiśniewska, M. The temperature effect on the adsorption mechanism of polyacrylamide on the silica surface and its stability. *Appl. Surf. Sci.* **2012**, *258*, 3094–3101. [CrossRef]

27. Wiśniewska, M.; Chibowski, S.; Urban, T.; Sternik, D.; Terpiłowski, K. Impact of anionic polyacrylamide on stability and surface properties of the Al(2)O(3)-polymer solution system at different temperatures. *Colloid Polym. Sci.* **2016**, *294*, 1511–1517. [CrossRef] [PubMed]

28. Mewis, J.; Wagner, N.J. *Colloidal Suspension Rheology*; Cambridge University Press: Cambridge, UK, 2011.

29. Farooq, U.; Tweheyo, M.T.; Sjöblom, J.; Øye, G. Surface Characterization of Model, Outcrop, and Reservoir Samples in Low Salinity Aqueous Solutions. *J. Dispers. Sci. Technol.* **2011**, *32*, 519–531. [CrossRef]

30. Sohal, M.A.; Thyne, G.; Søgaard, E.G. Review of Recovery Mechanisms of Ionically Modified Waterflood in Carbonate Reservoirs. *Energy Fuels* **2016**, *30*, 1904–1914. [CrossRef]

31. Blackman, L.D.; Gunatillake, P.A.; Cass, P.; Locock, K.E.S. An introduction to zwitterionic polymer behavior and applications in solution and at surfaces. *Chem. Soc. Rev.* **2019**, *48*, 757–770. [CrossRef] [PubMed]

32. Gan, Y.; Franks, G.V. Charging Behavior of the Gibbsite Basal (001) Surface in NaCl Solution Investigated by AFM Colloidal Probe Technique. *Langmuir* **2006**, *22*, 6087–6092. [CrossRef] [PubMed]

33. Gregory, J. Polymer adsorption and flocculation in sheared suspensions. *Colloids Surf.* **1998**, *31*, 231–253. [CrossRef]

34. Rasteiro, M.G.; Pinheiro, I.; Ahmadloo, H.; Hunkeler, D.; Garcia, F.A.P.; Ferreia, P.; Wandrey, C. Correlation between flocculation and adsorption of cationic polyacrylamides on precipitated calcium carbonate. *Chem. Eng. Res. Des.* **2015**, *95*, 298–306. [CrossRef]

35. Thomas, M.M.; Clouse, J.A.; Longo, J.M. Adsorption of organic compounds on carbonate minerals 1. Model compounds and their influence on mineral wettability. *Chem. Geol.* **1993**, *109*, 201–213. [CrossRef]

36. Al-Hashmi, A.R.; Luckham, P.F.; Heng, J.Y.Y.; Al-Maamari, R.S.; Zaitoun, A.; Al-Sharji, H.H.; Al-Wehaibi, T.K. Adsorption of High-Molecular-Weight EOR Polymers on Glass Surfaces Using AFM and QCM-D. *Energy Fuels* **2013**, *27*, 2437–2444. [CrossRef]

37. Plank, J.; Sachsenhauser, B. Impact of Molecular Structure on Zeta Potential and Adsorbed Conformation of .ALPHA.Allyl.OMEGA.-Methoxypolyethylene Glycol-Maleic Anhydride Superplasticizers. *J. Adv. Concr. Technol.* **2006**, *4*, 233–239. [CrossRef]

38. Hue, K.Y.; Lew, J.H.; Myo Thant, M.M.; Matar, O.K.; Luckham, P.F.; Müller, E.A. Molecular Dynamics Simulation of Polyacrylamide Adsorption on Calcite. *Molecules* **2023**, *28*, 6367. [CrossRef]

39. Xiong, B.; Zydney, A.L.; Kumar, M. Fouling of microfiltration membranes by flowback and produced waters from the Marcellus shale gas play. *Water Res.* **2016**, *99*, 162–170. [CrossRef]

40. Xiong, B.; Loss, R.D.; Shields, D.; Pawlik, T.; Hochreiter, R.; Zydney, A.L.; Kumar, M. Polyacrylamide degradation and its implications in environmental systems. *Npj Clean Water* **2018**, *1*, 17. [CrossRef]
41. LoPachin, R.M. The Changing View of Acrylamide Neurotoxicity. *NeuroToxicology* **2004**, *25*, 617–630. [CrossRef] [PubMed]